Journal of Materials Chemistry A

Accepted Manuscript

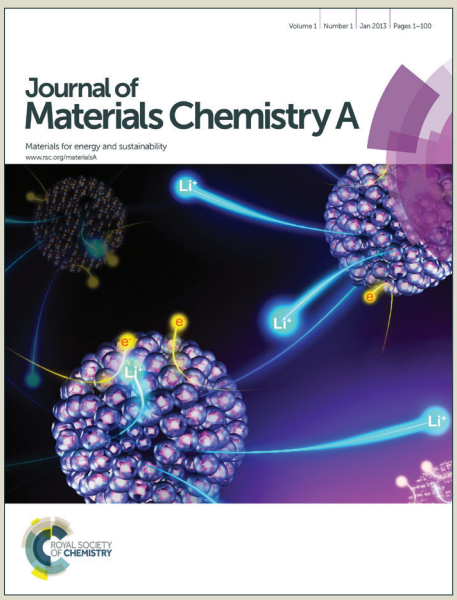

ROYAL SOCIETY OF CHEMISTRY

www.rsc.org/materialsA

Journal Name

RSCPublishing

ARTICLE

Lithium Reaction Mechanism and High Rate Capability of VS_4-Graphene Nanocomposite for Lithium Battery Anode Material

Cite this: DOI: 10.1039/x0xx00000x

Received 00th January 2012,
Accepted 00th January 2012

DOI: 10.1039/x0xx00000x

www.rsc.org/

Xiaodong Xu,[a†] Sookyung Jeong,[a†] Chandra Sekhar Rout,[a] Pilgun Oh,[a] Minseong Ko,[a] Hyejung Kim,[a] Min Gyu Kim,[b] Ruiguo Cao,[a] Hyeon Suk Shin[a*] and Jaephil Cho[a*]

Graphene-attached VS_4 composite prepared by a simple hydrothermal method is studied in terms of lithium reaction mechanism and high rate capability. The nanocomposite exhibits good cycling stability and impressive high-rate capability of lithium storage. The nanocomposite exhibits good cycling stability and impressive high-rate capability of lithium storage, delivering the comparable capacity of 630 and 314 mAh g^{-1} at even higher rates of 10 and 20 C (=10 and 20 A g^{-1}, or 10 and 20 mA cm^{-2}). In addition, a full-cell ($LiMn_2O_4$/VS_4-graphene) test result also exhibited good capacity retention. The mechanism of Li storage is systematically studied and a conversion reaction with irreversible phase change during the initial discharge-charge process is proposed.

Introduction

Recently, R & D activities in flexible energy storage system for wearable devices have been soaring and this storage system (batteries) requires high capacity and rate performance that allow the devices to be operated for long time and charged in a short time. As one of the leading candidates in the flexible batteries, Li-ion batteries (LIBs) have been widely considered, and the main challenge to realize the requirements is to design reliable electrodes with flexible property and high electrochemical performance. To approach toward flexible LIBs, graphene based composites are very promising in energy storage system because graphene can offer a large surface area providing more electrochemical reaction active sites and highly electron conductive network with superior mechanical flexibility.[1] For example, transition metal oxides and sulphides such as Fe_3O_4,[2] Co_3O_4,[3] MnO_2,[4] WS_2,[5-7] ZrS_2[8] and FeS[9] have been incorporated with graphene sheets to prepare flexible electrodes, which exhibited a high electrochemical performance due to that graphene plays a key role of the rapid electron transport and buffering role of volume expansion. Among them, MoS_2 material with sandwich-like layered structure is the most investigated one owing to its outstanding electrochemical performance and easy synthesis.[10] MoS_2 with different morphologies and sizes, and many kinds of MoS_2 composites, have been employed as anode materials for LIBs, exhibiting high capacity and good rate capability.[10-17] Comparable energy density (>100 Wh/Kg) was also reported for MoS_2 because of its high specific capacity, showing a great potential for LIBs.[18]

On the other hand, only a few papers reported the studies on utilizing vanadium sulfides and analogues for LIBs. The intercalation behaviour of Li^+ into VS_2 was investigated by Murphy et al., and VS_2 was then tested as cathode material.[19, 20] Murugan et al. expanded the interlayer spacing of VS_2 by in situ oxidative polymerization of 3,4-ethylenedioxythiophene (EDOT) and also tested it as cathode material for LIBs.[21] $VSe_{2-y}S_y$ and $Li_{0.8}VS_2$ have been tested as anode materials,[22, 23] showing capacity lower than 200 mAh g^{-1}. However, another vanadium sulfide, VS_4 has never been reported for usage in lithium storage due to the difficulty in the synthetic method, and only its crystallographic structure was reported so far.[24,25] Recently, we succeeded to prepare VS_4-loaded the reduced graphene (rGO) composite via simple hydrothermal process.[25]

Herein, we investigate Li reaction mechanism with VS_4-reduced graphene (VS_4-rGO) nanocompostie and high rate capability and cycling performance.

Experimental

Synthesis of VS_4-rGO composites

The synthesis of VS_4-rGO composites was followed in ref. 25. Graphene oxides (GO) was prepared from natural graphite powder by a modified Hummers' method.[25, 26] To prepare VS_4-rGO composite, 1.84 g (0.01 mol) of sodium orthovanadate (Na_3VO_4, Sigma-aldrich, 99.98%) and 3.75g (0.05 mol) of thioacetamide (C_2H_5NS, Sigma-Aldrich, ≥99%) were dissolved in 320 mL of DI water. Then 80 mL of GO solution (~5 mg/mL) was added. The mixture was stirred for 1 h at room temperature by using a magnetic stirrer. After getting homogenous solution, the mixture was transferred to a 500 mL

Teflon-lined stainless steel autoclave, sealed tightly and hydrothermal reaction was carried out at 160 °C for 24 h. After cooling naturally, the product was collected by filtration and washed with DI water and dried in vacuum at 60 °C for 6 h. During the hydrothermal process, VS_4 was formed on GO and GO was transformed to rGO. Besides, only rGO was obtained via the hydrothermal reaction of GO solution under the same condition but without addition of Na_3VO_4 and C_2H_5NS. For the synthesis of reference VS_4-10 wt% CNT composite sample, refer to supporting information.

Characterization of the Materials

Powder X-ray diffraction (PXRD) patterns were obtained on a High Power X-Ray Diffractometer (Rigaku) by using Cu-Kα radiation or Synchrotron Beamline Diffractometer (Pohang Accelerator Lab, Pohang, Korea). All the samples were sealed in tape before measurement to prevent them from oxidation. TEM and EDS mapping images were obtained by using JEM-2100 transmission electron microscope (JEOL) operated at 200kV. Mass spectra of pristine and cycled samples were obtained by using a Bi^+ beam on TOF-SIMS spectrometer (ION TOF) at an operating pressure of $< 5.0\times10^{-10}$ torr. Elemental analysis was performed on Flash2000 element analyzer (Thermo Scientific).

Electrochemical Characterization of the Materials

The anodes were made of VS_4-rGO or VS_4-CNT composite, Ketjen Black, and polyvinylidone fluoride (PVDF) binder (LG Chem.) in a weight ratio of 80:10:10. The coin-type half cells (2016R) were assembled in an Ar-filled glove box, using lithium metal foil as the counter electrode, microporous polyethylene as the separator, and 1.1 M $LiPF_6$ in ethylene carbonate/diethylene carbonate (EC/DEC, 1:1 in volume ratio, Panax Starlyte, Korea) as the electrolyte. The loading amount of the electrode material was measured as > 1 mg cm^{-2}. The coin-type full cell (2032R) was made of $LiMn_2O_4$ cathode and VS_4-rGO anode with N/P ratio of 1.1, and 1.1 M $LiPF_6$ in ethylene carbonate/ethyl methyl carbonate (EC/EMC, 3:7 in volume ratio, with 2% vinylene carbonate additive) was used as electrolyte. The capacity of a full-cell was ~1 mAh. The cell tests were performed with a WBCS3000 automatic battery cycler system at 23 °C, and the capacity was estimated based only on active materials (VS_4-rGO in half-cell, or VS_4-rGO and $LiMn_2O_4$ in full-cell). Cyclic voltammetry and electrochemical impedance spectroscopy (EIS) were carried out on an Ivium-n-Stat Multichannel Electrochemical Analyser (Ivium Technologies), using three-electrode cells with lithium metal as the counter and reference electrodes. The cyclic voltammogram (CV) was obtained in the voltage range of 0-3.0 V (vs. Li^+/Li) at a scan rate of 0.5 mV/s. The Nyquist plots were recorded by applying an AC voltage of 5 mV amplitude in the frequency range of 0.05 Hz to 100 kHz. All electrochemical measurements were carried out at room temperature.

Results and discussion

As-prepared VS_4 phase was confirmed by powder X-ray diffraction, and all the diffraction peaks can be assigned to VS_4 with a body-centered monoclinic phase (I2/c space group, a=6.77 Å, b =10.42 Å, c =12.11 Å, JCPDS card No. 87-0603). VS_4 could be described as $V^{4+}(S_2^{2-})_2$ **(Fig. S1A)**. It is a linear-chain compound with alternating bonding and nonbonding contacts between the octa-coordinated vanadium centers, and each S_2^{2-} unit bridges two neighboring vanadium atoms **(Fig. S1B)**.[27] No peak of rGO appeared in the XRD pattern, and elemental analysis showed the content of rGO in this composite was only ~3 wt%. SEM and TEM images confirmed that the composite consists of rGO-attached VS_4 nanorods, with sizes of ~200-300 nm in length and ~80-150 nm in width **(Fig. S2A, B)**, which agrees with the previous result.[25] The presence of agglomeration is believed to be caused by the interaction between VS_4 and rGO. HR-TEM image exhibits a typical layered structure, with an interlayer distance of 0.56 nm corresponding to the (110) plane of VS_4 **(Fig. 2SC)**. EDS mapping images further reveal the homogeneous distribution of vanadium and sulfur in the nanoparticles (Fig. S3).

Fig. 1A shows the representative cyclic voltammogram (CV) of VS_4-rGO measured in the voltage range of 0-3.0 V (vs. Li^+/Li) at a scan rate of 0.5 mV/s during the first three cycles. Reduction peaks attributed to the lithiation process at ~1.6, ~1.4 and ~0.6 V, and oxidation peaks corresponding to the de-lithiation process at ~1.8 and 2.4 V were observed in the first cycle, respectively. Two reduction peaks at ~1.6 and ~1.4 V might be related to the lithium insertion into VS_4 phase ($VS_4 \rightarrow Li_xVS_4$), and the peak at ~0.6 V may be originated from the decomposition of Li_xVS_4 to Li_2S and elemental V, based on the previous report on MoS_2.[10] The reduction peaks at ~1.6 and ~1.4 V shifted positively, while the peak at ~0.6 V disappeared in the following second and third cycles. **Fig. 1B** shows the typical discharge-charge voltage profiles of the composite within a cut-off voltage window of 0.01-3.0 V at a current rate of 0.05 C (1 C=1000 mA g^{-1}) in coin-type lithium half-cell (2016R) at 23 °C. The initial discharge and charge capacities were 1814 and 1170 mAh g^{-1}, respectively. The low Coulombic efficiency (CE) of 65% may be caused by the irreversible capacity loss, including inevitable decomposition of electrolyte and formation of solid electrolyte interface (SEI), which is common in transition metal oxides and sulfides based anode materials.[6, 12, 13, 28] The CE was greatly improved after the formation cycle, achieving 94% and 96% during the 2nd and 3rd cycles, with high charge capacities of 1161 and 1153 mAh g^{-1}, respectively. The 1st discharge profile is obviously different from the latter ones. Three potential plateaus at ~1.8 V, ~1.6 V and ~0.7 V are observed in the 1st discharge process, but only one potential plateau at ~2.1 V can be seen clearly during the 2nd and 3rd discharge. All of the three charge profiles seem to be similar to each other and two potential plateaus at ~1.8 V and ~2.4 V are observed. Such a variation can be seen more clearly from the differential curves during the first three cycles **(Fig. 1C)**. The obvious difference between CV curves and voltage profiles of the 1st and 2nd discharge processes indicated an irreversible phase transition during the 1st discharge-charge process. Similar phenomenon was found in other transition metal sulfides,[5, 10, 13, 29] among which the lithium storage mechanism of MoS_2 has been studied recently.[30]

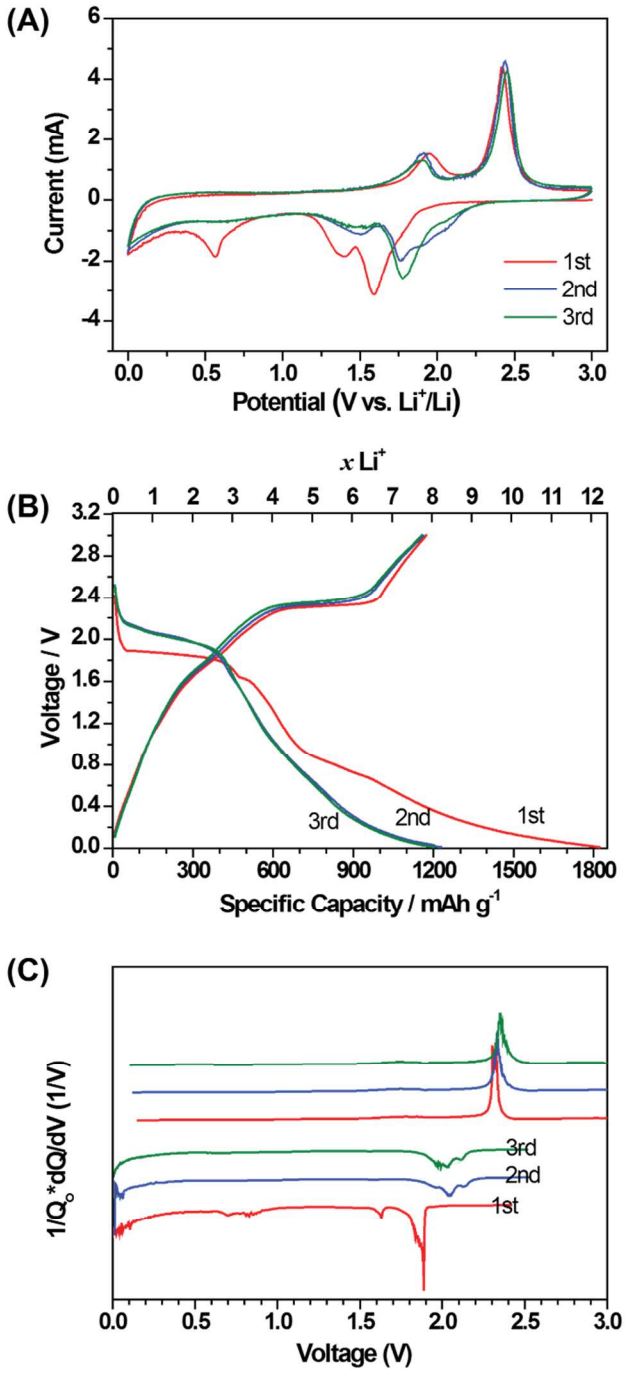

Fig. 1 (A) Cyclic voltammogram of VS_4-rGO measured in the voltage range of 0-3.0 V (vs. Li^+/Li) at a scan rate of 0.5 mV/s during the first three cycles. (B) Discharge-charge voltage profiles of VS_4-rGO at a current rate of 0.05 C in coin-type lithium cell (2016R) at 23 °C (1 C = 1000 mA g^{-1}). (C) Corresponding differential capacity curves during the first three cycles.

Fig. 2 shows the ex-situ XRD patterns of VS_4-rGO anodes after discharging or charging to different voltages at 0.1 C. The pristine electrode **(Fig. 2-a)** showed a consistent XRD pattern with VS_4-rGO powder. The two main peaks of VS_4 at ~15.8° and ~17.0° were remained at the first voltage plateau during discharge **(Fig. 2-b and c)**. This result is in accordance with the intercalation of 3 Li^+ ions at the first step of discharge (Li_3VS_4). Similar ternary alkali tetrathiovanadates such as Li_3VS_4·2DMF (in solution), K_3VS_4 and Na_3VS_4, have been reported previously.[31-33] The peak at ~15.8° disappeared after discharged to 1.65 V **(Fig. 2-d)**, indicating the decomposition of Li_3VS_4. The peak at ~17.0° also disappeared after further discharged to 0.5 V **(Fig. 2-e)** while new peak attributed to Li_2S (220) appeared at ~44.8°. Two weak peaks at ~41.2° and ~47.9° can be indexed to the (111) and (200) planes of V. The intensity of above peaks of Li_2S and V increased after fully discharged to 0.01 V, and another weak peak of Li_2S (311) at 53.1° was found **(Fig. 2-f)**. The main peaks of VS_4 did not appear again when finally charged to 3 V **(Fig. 2-g)**, demonstrating the irreversible phase transition during the initial discharge-charge process. The broad peak between 14-26° came from the tape.

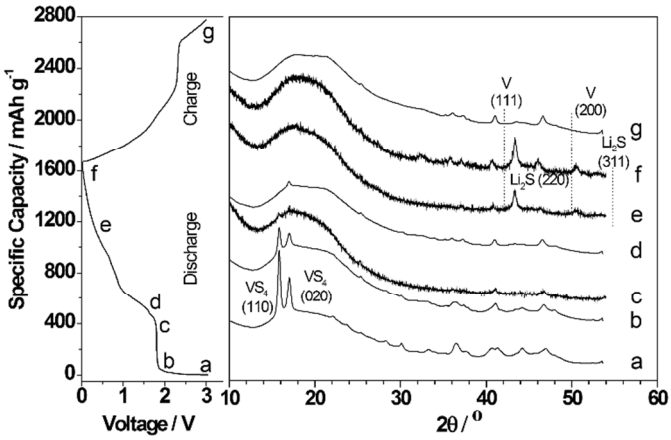

Fig. 2 Ex-situ XRD patterns obtained from VS_4-rGO anodes after discharging or charging to different voltages at 0.1 C: (a) pristine electrode (b-f) discharging to 2.00, 1.80, 1.65, 0.50 and 0.01 V (g) charging to 3 V.

TEM and EDS mapping were adopted to analysis the fully discharged and charged VS_4-rGO electrodes for further understanding the mechanism of lithium storage. Two different kinds of particles were seen in the fully discharged electrode **(Fig. 3A)**, and EDS mapping clearly revealed that elements of V and S were distributed in different particles. The solid and dense particle included only V. It should be nanosized metallic vanadium. The other S-rich particle with porous nature should be Li_2S, the most common fully discharged product of transition metal sulfides. HR-TEM image of the fully discharged product also showed d-spacing of 0.333 nm and 0.208 nm, which corresponded to the (111) and (220) planes of Li_2S **(Fig. 3A-inset)**. The re-formation of VS_4 did not happen after charging to 3 V. The nanosized metallic vanadium still existed in the fully charged VS_4-rGO electrode **(Fig. 3B)**, indicating its inert nature during the charge process. The porous Li_2S nanoparticle was converted to sulfur, which uniformly distributed in the whole area owing to the interaction between rGO and S. HR-TEM image of the S-rich region showed amorphous state **(Fig. 3B-inset)**, which is consistent with the absence of sulfur's peaks in XRD patterns.

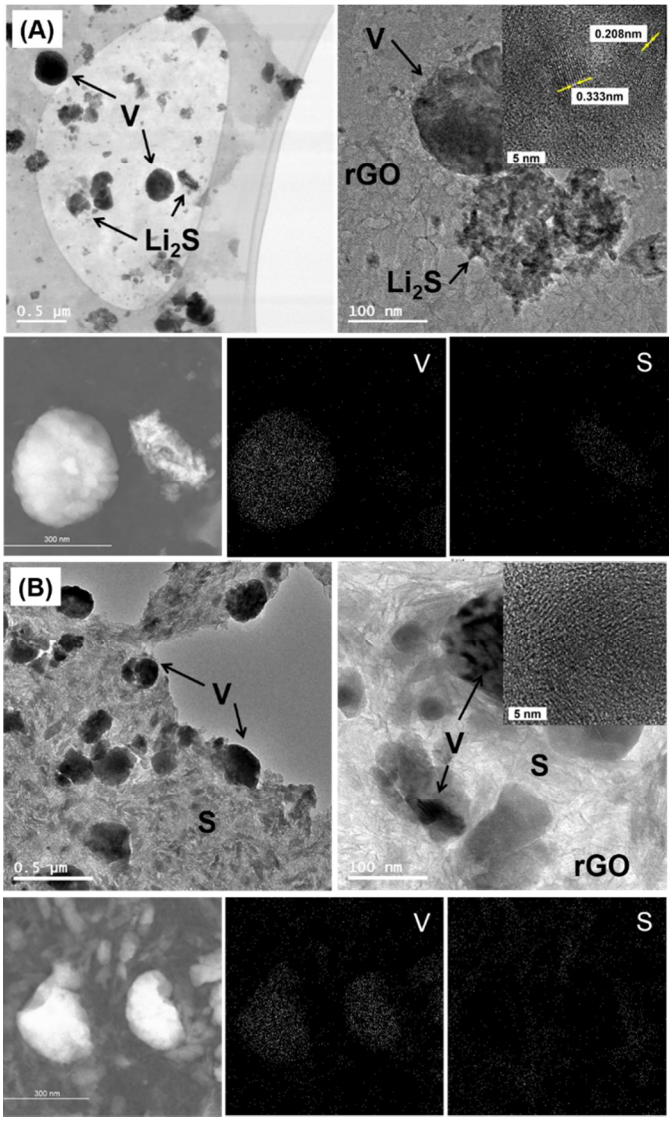

Fig. 3 TEM and EDS mapping images of (A) fully discharged electrode (inset: d-spacing of 0.333 and 0.208 nm corresponding to (111) and (220) plane, separately) and (B) fully charged electrode (inset: S-rich regions with amorphous state) of VS_4-rGO at 0.1 C (1 C = 1000 mA g^{-1}).

The intrinsic electronic conductivity of cells could be improved owing to the generation of metallic vanadium during cycling. The electrochemical impedance of VS_4-rGO based coin-type lithium cell was measured before and after cycling **(Fig. 4A)**. The Nyquist plot shows a semicircle with large diameter at high frequencies before discharge-charge, indicating high resistance at the interface. The depressed semicircle with reduced diameter at high frequencies suggests decreased impedance after cycling, because of the presence of vanadium metal. A similar result has also been reported in MoS_2 based electrode.[13] Time-of-Flight Secondary Ion Mass Spectrometry (TOF-SIMS) was also employed to analysis the composition of electrode after discharge and charge. The mass spectra of pristine electrode show the peaks of VS^+ and VS^{4+} cations **(Fig. 4B and C)**. However, these peaks disappeared after discharging to 0.01 V and charging to 3 V, also denying the re-formation of VS_4.

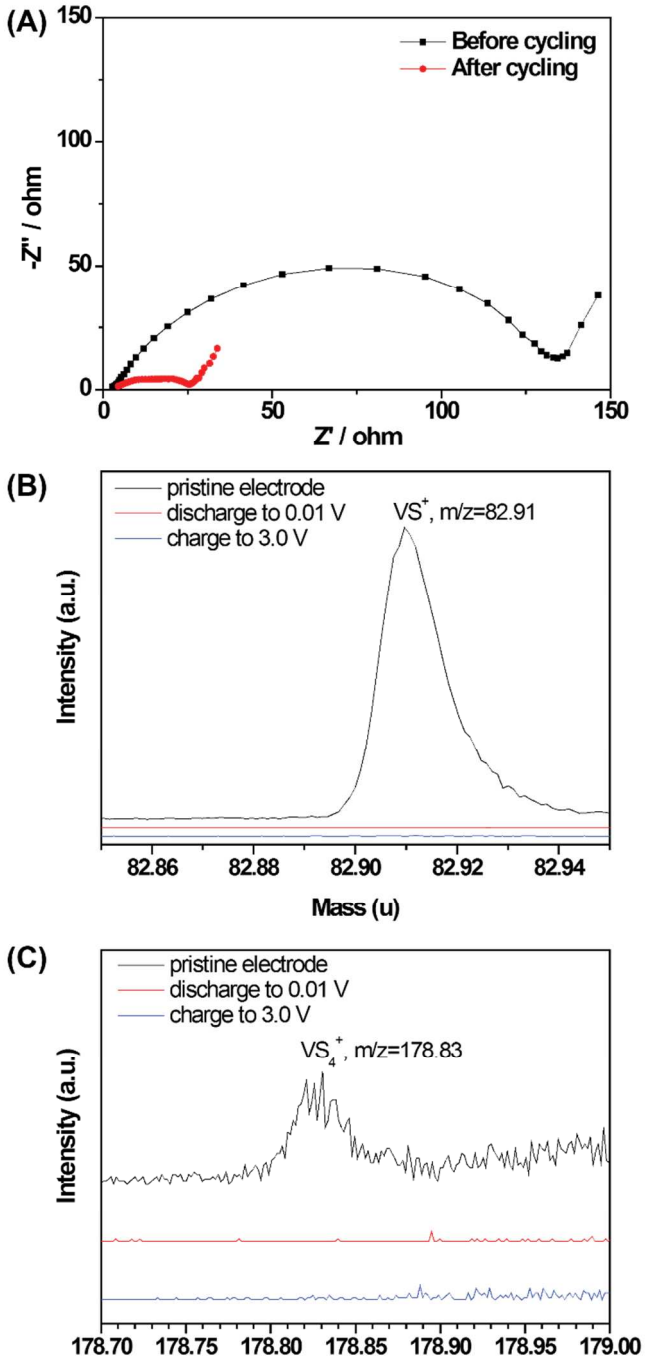

Fig. 4 (A) Nyquist plot of VS_4-rGO based coin-type lithium ion cell (2016R) before and cycling. (B and C) TOF-SIMS spectra of VS_4-rGO composite electrode before and after discharge-charge.

In consequence, we propose a possible lithium storage mechanism of VS_4-rGO composite as follows:
An initial discharge:

$$VS_4 + 3Li^+ + 3e^- \rightarrow Li_3VS_4 \text{ (Above 1.7 V)} \quad (1)$$

$$Li_3VS_4 + 5Li^+ + 5e^- \rightarrow 4Li_2S + V \text{ (0.01 V)} \quad (2)$$

Followed by

$$Li_2S \leftrightarrow S + 2Li^+ + 2e^- \text{ (Below 3 V)} \quad (3)$$

Intercalation of 3 Li^+ ions occurred first in the initial discharge, followed by the decomposing of Li_3VS_4 to Li_2S and V after further discharging to 0.01 V. Then, Li_2S was converted to S after charging to 3 V, while metallic vanadium remained inert. This is quite different from most transition metal oxides, and might be due to the weaker oxidation capability of sulfur than that of oxygen.[30] After that, the electrochemical reaction just happened between S and Li_2S during the next cycles. There should be 8 Li^+ ions involved for each VS_4 based on the above mechanism, and a much higher theoretical capacity can be achieved from VS_4 in comparison to MoS_2 and other transition metal sulfides. The theoretical capacity of VS_4 could be calculated as 1196 mAh g^{-1}, which is very close to the first charge capacity of 1170 mAh g^{-1} at 0.05 C. On the other hand, the conversion mechanism of VS_4 has not been fully verified owing to the difficulty in characterization, and further studies are still needed to explain it in details.

The cycling performance of VS_4-rGO composite at a high current rate of 4 C (=4 A g^{-1}) between 0.01 and 3.0 V was tested after an initial formation cycle at 0.1 C **(Fig. 5)**. The composite electrode delivered a high charge capacity of 820 mAh g^{-1} with a high CE of 96%. The reversible capacity still remained 727 mAh g^{-1} after 50 cycles, which is 89% of the initial capacity. Such high capacity-retention of transition metal sulfides or their composites at high current rates is few reported, although good cycling stability was achieved at much lower current densities from MoS_2, ZrS_2, WS_2, etc.[7, 8, 11, 12, 15, 34] Furthermore, the CE was maintained at 99% after the 5th cycle. The capacity contribution of rGO was also evaluated, and the specific capacity of rGO was found to be lower than 160 mAh g^{-1} at the same current rate **(Fig. S4)**. Therefore, its contribution to the total capacity could be negligible while there was only 3 wt% of rGO in the composite.

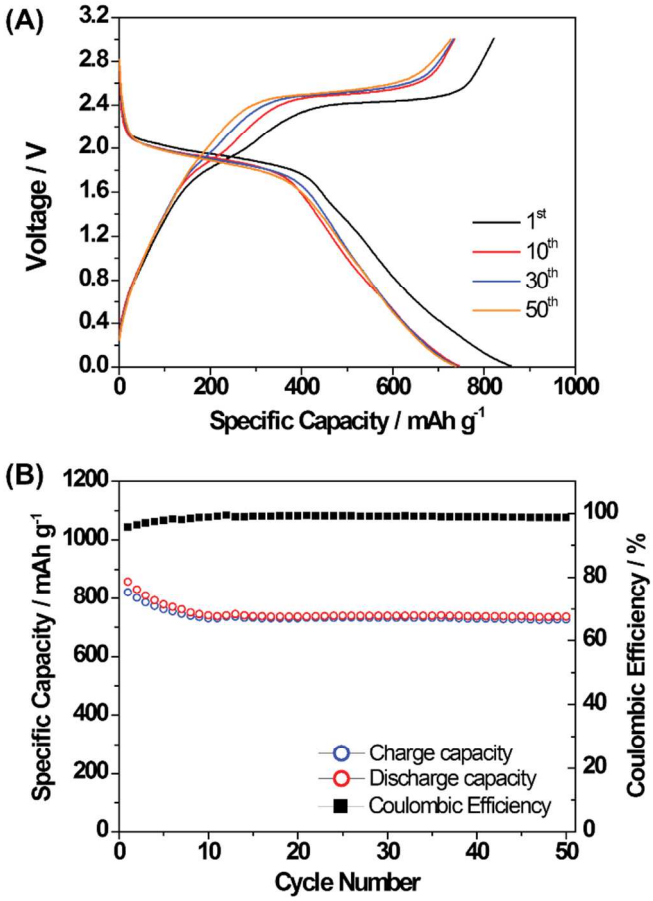

Fig. 5 (A) Voltage profiles of VS_4-rGO at a current rate of 4 C in coin-type lithium cell (2016R) at 23 °C. (B) Cycling performance of VS_4-rGO at 4 C (1 C = 1000 mA g^{-1}). An initial formation cycle at a low current rate of 0.1 C was applied before the discharge-charge cycling at 4 C rate.

For the comparison of lithium storage capability with VS_4-rGO, VS_4-10 wt% carbon nanotube (VS_4-10CNT) was synthesized **(Fig. S5)** and evaluated its electrochemical performance. The electrochemical performance is highly related to the dispersion of active materials on the electron conduction matrix. In contrast to VS_4-10CNT (Figure S2), CNT in CNT/VS_4 composites does not give insufficient coverage with VS_4, resulting in a decrease of effective electron transport pathway between the VS_4 nanoparticles. It is therefore reasonable to conclude that rGO-based sample showed better performance than CNT-based one. **Figure 6** showed superior rate capability of the VS_4-rGO composite. VS_4-rGO and VS_4-10CNT delivered a charge capacity of 913 and 733 mAh g^{-1} at 2 C rate, respectively, showing much higher capacity retention than the VS_4-10CNT (**also see Fig. S6**). Especially, the reversible capacity of VS_4-rGO remained as high as 630 and 314 mAh g^{-1} when the rate was increased to 10 C (=10 A g^{-1}, or 10 m Acm^{-2}) and 20 C (=20 A g^{-1}, or 20 mA cm^{-2}), respectively. Such a remarkable high-rate performance is superior to that of most transition metal sulfides based electrodes previously reported,[7-9, 11-17] and the results was induced by the special 2D structure of rGO, giving a large surface area and the strong interaction between the active materials and rGO.[35, 36] In addition,

Considering its application as anode material in LIBs, the high charge-discharge voltage plateau (~2.4 V) of VS_4/rGO might be a disadvantage. However, $Li_4Ti_5O_{12}$ and MoS_2, which also exhibit high voltage plateaus, have been widely reported as anode materials for LIBs. VS_4 delivers a much higher capacity in comparison to $Li_4Ti_5O_{12}$ (1196 mAh g^{-1} vs. 175 mAh g^{-1}) although its potential is also higher than that of $Li_4Ti_5O_{12}$, so a comparable energy density can still be expected for VS_4. In addition, recently there are many R & D activities to develop anode materials with high capacity and high rate capability for LIBs in regenerative break system of electric vehicles (EVs). For instance, one candidate is $Li_4Ti_5O_{12}$ anode and $LiFePO_4$ cathode with a voltage plateau of <2V.[37, 38] $Li_4Ti_5O_{12}$-$LiFePO_4$ battery system was also reported for its application in stationary energy storage and smart textiles.[39, 40] In this regard, opportunities may still exist to employ VS_4/rGO as the anode if paired with a high voltage (>4 V) cathode, while considering its high capacity and especially the impressive rate capability.

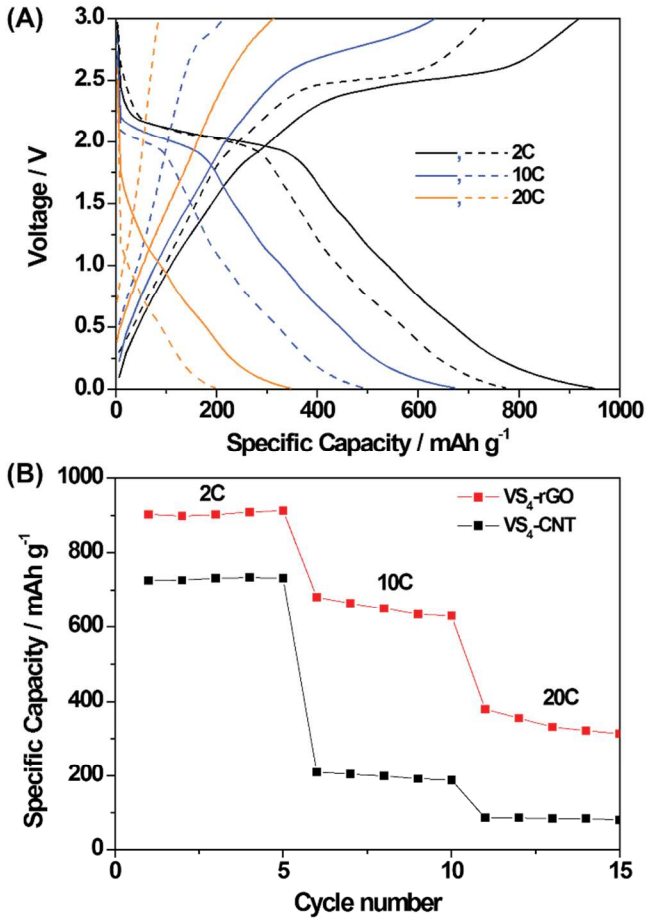

Fig. 6 (A) Voltage profiles of VS_4-rGO and VS4-10 wt% CNT at different current rates in coin-type lithium cell (2016R) at 23 °C (solid line: VS_4-rGO, dash line: VS_4-10 wt% CNT). (B) Rate performance with increasing charge rate from 2 to 20 C. The discharge rate is fixed at 0.1 C (1 C = 1000 mA g^{-1}).

To prove this point, we carried out preliminary full-cell test consisting of $LiMn_2O_4$ cathode and VS_4-rGO anode in a coin-type full-cell (2032R) between 4.3 and 1.0 V at 0.5 C under 23 °C **(Fig. 7)**. The specific capacity is estimated based on sole amount of the active material. The first discharge capacity was 72 mAh g^{-1}, and comparable capacity retention of 74% was achieved after 30 cycles. A better performance could be expected after further optimization of the full-cell configuration. The main text of the article should go here with headings as appropriate.

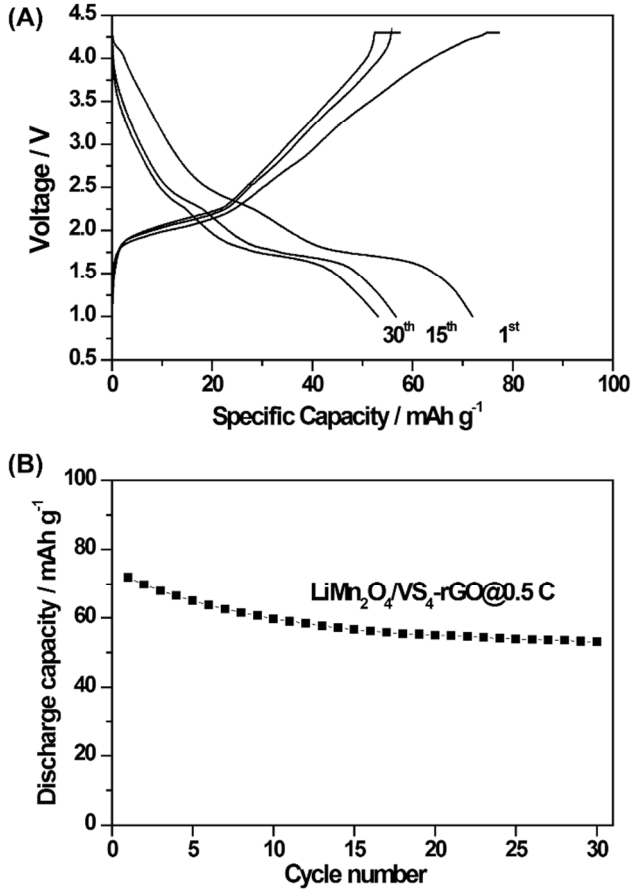

Fig. 7 (A) Voltage profiles of $LiMn_2O_4$/VS_4-rGO in a coin-type full-cell (2032R) between 4.3 and 1.0 V at a rate of 0.5 C after the formation cycle at 0.1 C. (B) Corresponding discharge capacity as a function of cycle number.

Such outstanding electrochemical performance of VS_4-rGO could be attributed to the following reasons. First, the existence of rGO improved both the conductivity and stability of VS_4-rGO electrode, which may bring better cycling stability and rate capability. Second, although V did not participate in the electrochemical reaction after the initial discharge, the nanosized metallic V enhanced the electronic conductivity of the Li_2S/V or S/V composite during the following discharge-charge process. In addition, the dissolution of polysulfide, which is common in Li-sulfur batteries, could be possibly depressed owing to the absorption effect of the nanosized V with high surface energy.[13, 30, 41, 42]

Conclusions

In summary, we have prepared graphene-attached VS_4 nanorods by a simple hydrothermal method. This VS_4-rGO composite exhibited good cycling stability and impressive high-rate capability of lithium storage in half-cell, and the full-cell test has also demonstrated the possibility of using VS_4-rGO as

anode paired with a high-voltage cathode in LIBs despite of its high lithiation voltage. In comparison to other transition metal sulfides, VS_4 is a more promising material for LIBs, owing to its much higher theoretical capacity as well as good cycling stability and excellent high-rate capability. Further studies on VS_4 with more efforts may accelerate the development of transition metal sulfides for LIBs while considering its outstanding performance. In addition, the mechanism of Li storage for VS_4 was also systematically studied for the first time, which would also be very useful in further research on transition metal sulfides for LIBs.

Acknowledgements

This work was supported by the Converging Research Center Program (2013K000210) and Center for Advanced Soft Electronics (Code No. 2011-0031630) under the Global Frontier Research Program through the National Research Foundation funded by MEST of Korea.

Notes and references

[a] School of Energy and Chemical Engineering, Ulsan National Institute of Science and Technology (UNIST), Ulsan, 689-798 (Korea). E-mail: shin@unist.ac.kr, jpcho@unist.ac.kr

[b] Beamline Research Division, Pohang Accelerator Laboratory, Pohang, 790-784 (Korea)

† These authors contributed equally to this work.

Electronic Supplementary Information (ESI) available: See DOI: 10.1039/b000000x/

1 G. Zhou, F. Li, H.-M. Cheng, *Energy Environ. Sci.* 2014, DOI: 10.1039/C3EE43182G.
2 R. Wang, C. Xu, J. Sun, L. Gao, C. Lin, *J. Mater. Chem. A* 2013, **1**, 1794.
3 R. Wang, C. Xu, J. Sun, Y. Liu, L. Gao, C. Lin, *Nanoscale* 2013, **5**, 6960.
4 A. Yu, H. W. Park, A. Davies, D. C. Higgins, Z. Chen, X. Xiao, *J. Phys. Chem. Lett.* 2011, **2**, 1855.
5 G. X. Wang, S. Bewlay, J. Yao, H. K. Liu, S. X. Dou *Electrochem. Solid State Lett.* 2004, **7**, A321.
6 C. Feng, L. Huang, Z. Guo, H. Liu, *Electrochem. Commun.* 2007, **9**, 119.
7 H. Liu, D. Su, G. Wang, S. Z. Qiao, *J. Mater. Chem.* 2012, **22**, 17437.
8 J.-t. Jang, S. Jeong, J.-w. Seo, M.-C. Kim, E. Sim, Y. Oh, S. Nam, B. Park, J. Cheon, *J. Am. Chem. Soc.* 2011, **133**, 7636.
9 C. Xu, Y. Zeng, X. Rui, N. Xiao, J. Zhu, W. Zhang, J. Chen, W. Liu, H. Tan, H. H. Hng, Q. Yan, *ACS Nano* 2012, **6**, 4713.
10 H. Hwang, H. Kim, J. Cho, *Nano Lett.* 2011, **11**, 4826.
11 G. Du, Z. Guo, S. Wang, R. Zeng, Z. Chen, H. Liu, *Chem. Commun.* 2010, **46**, 1106.
12 K. Chang, W. Chen, *ACS Nano* 2011, **5**, 4720.
13 J. Xiao, X. Wang, X.-Q. Yang, S. Xun, G. Liu, P. K. Koech, J. Liu, J. P. Lemmon, *Adv. Funct. Mater.* 2011, **21**, 2840.
14 K. Chang, W. Chen, *Chem. Commun.* 2011, **47**, 4252.
15 H. Liu, D. Su, R. Zhou, B. Sun, G. Wang, S. Z. Qiao, *Adv. Energy Mater.* 2012, **2**, 970.
16 X. Zhou, L.-J. Wan, Y.-G. Guo, *Nanoscale* 2012, **4**, 5868.
17 J.-Z. Wang, L. Lu, M. Lotya, J. N. Coleman, S.-L. Chou, H.-K. Liu, A. I. Minett, J. Chen, *Adv. Energy Mater.* 2013, **3**, 798.
18 R. Dominko, D. Arčon, A. Mrzel, A. Zorko, P. Cevc, P. Venturini, M. Gaberscek, M. Remskar, D. Mihailovic, Adv. Mater. 2002, **14**, 1531.
19 D. W. Murphy, J. N. Carides, F. J. Di Salvo, C. Cros, J. V. Waszczak, *Mater. Res. Bull.* 1977, **12**, 825.
20 D. W. Murphy, F. J. Di Salvo, J. N. Carides, *J. Solid State Chem.* 1979, **29**, 339.
21 A. Vadivel Murugan, M. Quintin, M.-H. Delville, G. Campet, K. Vijayamohanan, *J. Mater. Chem.* 2005, **15**, 902.
22 R. Guzma´N, P. Lavela, J. Morales, J. L. Tirado, *J. Appl. Electrochem.* 1997, **27**, 1207.
23 Y. Kim, K.-s. Park, S.-h. Song, J. Han, J. B. Goodenough, *J. Electrochem. Soc.* 2009, **156**, A703.
24 B. Pedersen, *Acta Chem. Scand.* 1959, **13**, 1050.
25 C. S. Rout, B.-H. Kim, X. Xu, J. Yang, H. Y. Jeong, D. Odkhuu, N. Park, J. Cho, H. S. Shin, *J. Am. Chem. Soc.* 2013, **135**, 8720.
26 N. I. Kovtyukhova, P. J. Ollivier, B. R. Martin, T. E. Mallouk, S. A. Chizhik, E. V. Buzaneva, A. D. Gorchinskiy, *Chem. Mater.* 1999, **11**, 771.
27 S. J. Hibble, R. I. Walton, D. M. Pickup, *J. Chem. Soc., Dalton Trans.* 1996, **0**, 2245.
28 J. Cabana, L. Monconduit, D. Larcher, M. R. Palacín, Adv. Mater. 2010, **22**, E170.
29 J. Xiao, D. Choi, L. Cosimbescu, P. Koech, J. Liu, J. P. Lemmon, *Chem. Mater.* 2010, **22**, 4522.
30 X. Fang, X. Guo, Y. Mao, C. Hua, L. Shen, Y. Hu, Z. Wang, F. Wu, L. Chen, *Chem. Asian J.* 2012, **7**, 1013.
31 Y. P. Zhang, R. H. Holm, *Inorg. Chem.* 1988, **27**, 3875.
32 P. D. a. W. Bensch, Eur. *J. Solid State Inorg. Chem.* 1996, **33**, 309.
33 K. O. K. a. G. Gabl, Eur. *J. Solid State Inorg. Chem.* 1997, **34**, 1143.
34 K. Chang, W. Chen, *J. Mater. Chem.* 2011, **21**, 17175.
35 J. Schuster, G. He, B. Mandlmeier, T. Yim, K. T. Lee, T. Bein, L. F. Nazar, *Angew. Chem. Int. Ed.* 2012, **51**, 3591.
36 S. Evers, L. F. Nazar, *Acc. Chem. Res.* 2012, **46**, 1135.
37 LG Chem. & Samsung SDI, and Hyndai Motors, private communications
38 A. Jaiswal, C. R. Horne, O. Chang, W. Zhang, W. Kong, E. Wang, T. Chern, M. M. Doeff, *J. Electrochem. Soc.* 2009, **156**, A1041.
39 W. Wang, D. Choi, Z. Yang, *Metall and Mat Trans A* 2013, **44**, 21.
40 Y. Liu, S. Gorgutsa, C. Santato, M. Skorobogatiy, *J. Electrochem. Soc.* 2012, **159**, A349.
41 J. Schuster, G. He, B. Mandlmeier, T. Yim, K. T. Lee, T. Bein, L. F. Nazar, *Angew. Chem. Int. Ed.* 2012, **51**, 3591.
42 S. Evers, L. F. Nazar, *Acc. Chem. Res.* 2012, **46**, 1135.